An Expedition on Alkali and Alkaline-Earth Isocyanurate Hydrates: Structure Elucidation, Thermogravimetry, and Spectroscopy

Peter Gross[a] and Henning A. Höppe*[a]

Dedicated to Professor Wolfgang Schnick on the Occasion of his 60th Birthday

Abstract. Several alkali and alkaline earth (iso)cyanurates were synthesized by simple aqueous acid-base reactions and aqueous salt metathesis reactions, respectively, yielding nine new structure types. Single-crystals could be grown and the crystal structures of $Rb[H_2C_3N_3O_3]\cdot H_2O$-I, $Rb[H_2C_3N_3O_3]\cdot H_2O$-II, $Cs[H_2C_3N_3O_3]\cdot 0.5H_2O$, $Sr[H_2C_3N_3O_3]_2\cdot 4H_2O$, $Ba_3[H_2C_3N_3O_3]_2[HC_3N_3O_3]_2\cdot 4H_2O$, $Ca[HC_3N_3O_3]\cdot 3.5H_2O$, $Sr[HC_3N_3O_3]\cdot 3H_2O$, $Sr[HC_3N_3O_3]\cdot 2H_2O$, and $Sr_2[C_3N_3O_3]OH$ were elucidated by single-crystal XRD. $Rb_3[H_2C_3N_3O_3]_3[H_3C_3N_3O_3]\cdot 4H_2O$, $Cs[H_2C_3N_3O_3]\cdot 0.5H_2O$, and $Sr[HC_3N_3O_3]\cdot 2H_2O$ were synthesized as phase pure, crystalline powders and were further characterized by powder XRD, FT-IR spectroscopy, UV/Vis spectroscopy, and thermogravimetry. $Sr[HC_3N_3O_3]\cdot 2H_2O$ was shown to be an air- and water-resistant, cheap and easily obtained precursor for the phase-pure synthesis of $Sr_3[C_3N_3O_3]_2$, a promising SHG material, and Sr[NCN]. Moreover, an interesting dependence of the polymeric anion structure from its protonation degree was observed.

Introduction

Recently, metal (iso)cyanurates received increasing attention[1–6] due to the discovery of the remarkable nonlinear optical (NLO) properties of some alkaline earth cyanurates[7] and the associated prospects for new *second-harmonic-generation* (SHG)-materials featuring cyanurate anions.[8] Frequently, the growth of sufficiently large single-crystals of such materials might be assisted by providing suited precursor compounds. In the light of these encouraging findings we took a closer look on the related and basically well-known class of alkali and alkaline earth isocyanurate hydrates[9] with an emphasis on their structural investigation and thermal decomposition.

Up to now, structural elucidation by diffraction methods has only been conducted for one rubidium,[10] three potassium,[11,12] one calcium[13,14] and nine transition metal compounds.[15–17] Nevertheless, these investigations already revealed a rich structural diversity caused and governed by reaction stoichiometry. Our goal is to broaden the scope of the so far limited knowledge of this compound class following the goal to systematize its crystal chemistry; moreover, we keep on searching for other possible SHG materials and potential precursors for such materials.[9] We investigated also the vibrational and absorption spectroscopic properties as well as the thermal decomposition of all compounds we obtained as phase pure powders.

Regarding alkali isocyanurates, we report the syntheses and crystal structures of two modifications of $Rb[H_2C_3N_3O_3]\cdot H_2O$ as well as of $Cs[H_2C_3N_3O_3]\cdot 0.5H_2O$. Spectroscopic and thermal properties of $Cs[H_2C_3N_3O_3]\cdot 0.5H_2O$ and $Rb_3[H_2C_3N_3O_3]_3[H_3C_3N_3O_3]\cdot 4H_2O$ are reported, the crystal structure of the latter was already described by *Nichol* et al.[10] Disappointingly, none of these structures were found to be non-centrosymmetric. With regard to alkaline earth (iso)cyanurates, we report the syntheses and crystal structures of $Sr[H_2C_3N_3O_3]_2\cdot 4H_2O$, $Ba_3[H_2C_3N_3O_3]_2[HC_3N_3O_3]_2\cdot 4H_2O$, $Ca[HC_3N_3O_3]\cdot 3.5H_2O$, $Sr[HC_3N_3O_3]\cdot 3H_2O$, $Sr[HC_3N_3O_3]\cdot 2H_2O$, and $Sr_2[C_3N_3O_3]OH$. $Sr[H_2C_3N_3O_3]_2\cdot 4H_2O$ is the only compound that might possibly feature a non-centrosymmetric crystal structure, though diffractometric indicators are rather ambiguous. $Sr[HC_3N_3O_3]\cdot 2H_2O$ is shown to be a cheap and robust precursor for Sr[NCN] and SHG-active $Sr_3[C_3N_3O_3]_2$ via simple thermal decomposition. Finally, we could prove for the first time by the synthesis of $Sr_2[C_3N_3O_3]OH$, that crystallization of tribasic metal cyanurates from aqueous solution is possible.

Results and Discussion

Synthetic Approaches

Alkali isocyanurates proved to be sufficiently soluble to be synthesized by a simple aqueous acid-base reaction from alkali carbonates and cyanuric acid with subsequent crystallization via slow evaporation. $Rb[H_2C_3N_3O_3]\cdot H_2O$ crystallizes at the probed synthesis-conditions simultaneously in

* Prof. Dr. H. A. Höppe
E-Mail: henning@ak-hoeppe.de
[a] Institut für Physik
Universität Augsburg
Universitätsstr. 1
86159 Augsburg, Germany
Supporting information for this article is available on the WWW under **http://dx.doi.org/10.1002/zaac.201700254** or from the author.

two modifications, termed $Rb[H_2C_3N_3O_3]\cdot H_2O$-I (**1**) and $Rb[H_2C_3N_3O_3]\cdot H_2O$-II (**2**), whereas for $Cs[H_2C_3N_3O_3]\cdot 0.5H_2O$ (**3**) only a single modification was found. The obtained mixtures of the two monobasic rubidium modifications were always additionally accompanied by $Rb_3[H_2C_3N_3O_3]_3[H_3C_3N_3O_3]\cdot 4H_2O$ (**4**), which was already mentioned in literature,[10] though the authors mentioned certain doubts regarding the correctness of their structure. The crystal structures of these compounds were determined by single-crystal X-ray diffraction. $Rb_3[H_2C_3N_3O_3]_3[H_3C_3N_3O_3]\cdot 4H_2O$ (**4**) and $Cs[H_2C_3N_3O_3]\cdot 0.5H_2O$ (**3**) could both be obtained as phase pure powders and were characterized by powder XRD, FT-IR spectroscopy, UV/Vis spectroscopy, and thermogravimetry.

In contrast to the alkali compounds, alkaline earth isocyanurate hydrates were found to show a very low solubility in water; they were therefore synthesized by aqueous salt metathesis employing solutions of the respective alkaline earth chloride and sodium cyanurate. Crystals of alkaline earth isocyanurates suitable for single-crystal XRD were grown via slow interdiffusion of the starting material solutions within an U-formed tube. The respective calcium (**5**: $Ca[H_2C_3N_3O_3]_2\cdot 7H_2O$, **6**: $Ca[HC_3N_3O_3]\cdot 3.5H_2O$) and strontium (**7**: $Sr[H_2C_3N_3O_3]_2\cdot 4H_2O$, **8**: $Sr[HC_3N_3O_3]\cdot 3H_2O$, **9**: $Sr_2[C_3N_3O_3]OH$) compounds crystallize from aqueous solutions depending on the pH of the mother liquor, roughly according to the compiled pK_a values of cyanuric acid.[18] A series of photos of the crystallization of **8** was recorded and rendered into a video, in order get an impression of the interdiffusion kinetics (available as Supporting Information). Typically, the obtained samples comprise mixtures of several phases differing in their degree of deprotonation and hydration. Under strongly basic conditions (pH $>$ 13), alkaline earth carbonates easily form and therefore CO_2 must be thoroughly excluded from the reaction vessel. Moreover, $Sr[HC_3N_3O_3]\cdot 2H_2O$ (**10**) could be obtained from **8** by dehydration in air. $Ba_3[H_2C_3N_3O_3]_2[HC_3N_3O_3]_2\cdot 4H_2O$ (**11**) forms readily from Ba^{2+} and isocyanurate containing solutions, independent from the pH of the mother liquor. The crystal structures of all compounds except $Ca[H_2C_3N_3O_3]\cdot 7H_2O$ (refer to the literature[13,14] for a discussion of its crystal structure) were elucidated by single-crystal XRD and are discussed below. $Sr[HC_3N_3O_3]\cdot 2H_2O$ was obtained as a phase pure sample and characterized further by powder XRD, FT-IR spectroscopy, UV/Vis spectroscopy and thermogravimetry.

$Rb[H_2C_3N_3O_3]\cdot H_2O$ (1 and 2)

$Rb[H_2C_3N_3O_3]\cdot H_2O$-I (**1**) crystallizes in its own structure type in the space group $P\bar{1}$ (no. 2). The crystal structure (Figure 1a) exhibits dibasic isocyanurate anions $[H_2O_3C_3N_3]^-$ (Figure 2a) with typical bond lengths (1.34–1.38 Å for C–N and 1.22–1.25 Å for C–O) and angles. Adjacent isocyanurate anions are almost coplanar with each other (dihedral angle: 1.8°, Figure S1a, Supporting Information). These anions are interconnected by strong hydrogen bonds[19] between the two protonated nitrogen atoms and two accepting carbonyl oxygen atoms to form flat, infinite ribbons, as shown in Figure 2b.

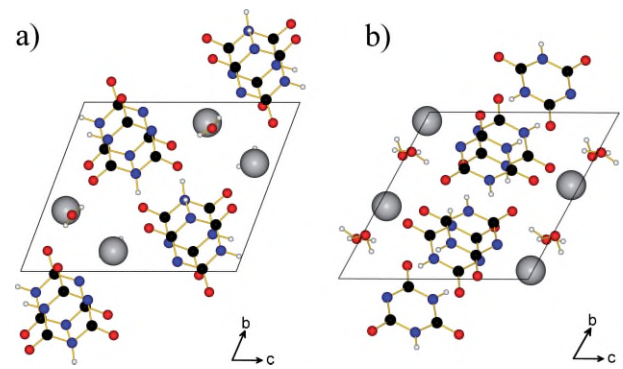

Figure 1. The unit cells of (a) $Rb[H_2C_3N_3O_3]\cdot H_2O$-I (**1**) and (b) $Rb[H_2C_3N_3O_3]\cdot H_2O$-II (**2**) viewed along [100] (Rb: grey spheres, C: black spheres, N: blue spheres, O: red spheres and H: white spheres, covalent bonds: yellow sticks).

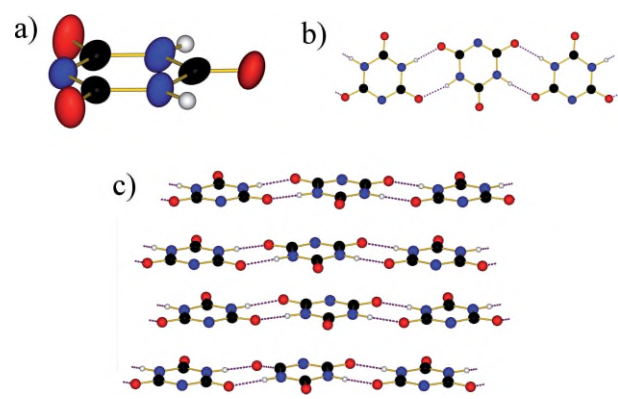

Figure 2. Ball-and-stick-model of the $[H_2C_3N_3O_3]^-$ anion in $Rb[H_2C_3N_3O_3]\cdot H_2O$-I (**1**) (hydrogen bonds: fragmented violet line). (a) Atoms shown as thermal anisotropic ellipsoids (50%). (b) Isocyanurate-ribbon depicted from top. (c) Layers resulting from stacked isocyanurate ribbons.

The ribbon motif is very often encountered, and it is present in all alkali[10–12] and 3d transition metal[14–17] isocyanurate structures hitherto found. These ribbons are stacked along [100] forming isocyanurate layers as shown in Figure 2c. In-between these layers there are layers comprising Rb^+ cations and water molecules (Figure 3a). The angle between the isocyanurate ribbons and Rb^+-H_2O layer amounts to approx. 78°. The water molecules connect adjacent isocyanurate layers via hydrogen bonds. The Rb^+ cations are situated on two crystallographic sites: Rb1 is surrounded by three carbonyl oxygen atoms, three deprotonated nitrogen atoms, and three water molecules forming a distorted tricapped trigonal prism (CN = 9), while Rb2 is surrounded by five carbonyl oxygen atoms and three water molecules, best described by a distorted bicapped trigonal prism (CN = 8), as shown in Figure 4. The interatomic distances between Rb and the surrounding atoms correspond on average (3.02 Å and 3.06 Å for CN = 8 and CN = 9, respectively) well with the sum of the ionic radii (2.99 Å and 3.01 Å).

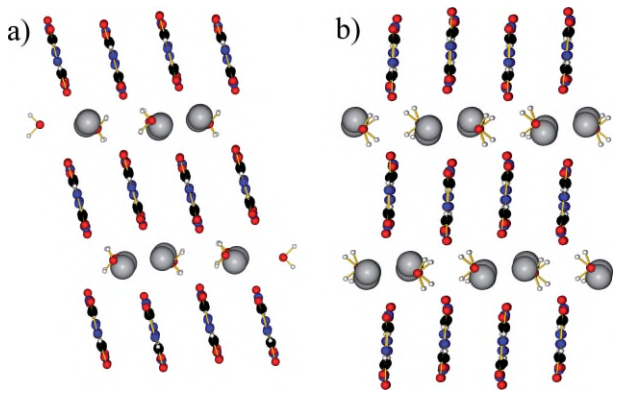

Figure 3. Layered structure of (a) $Rb[H_2C_3N_3O_3]\cdot H_2O$-I (**1**) and (b) $Rb[H_2C_3N_3O_3]\cdot H_2O$-II (**2**).

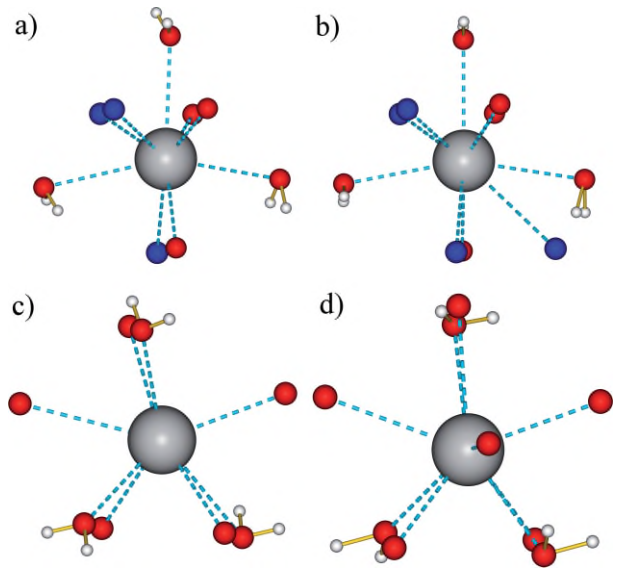

Figure 4. Coordination environment of the Rb positions in $Rb[H_2C_3N_3O_3]\cdot H_2O$-I (**1**) [(a) Rb1 and (c) Rb2] and $Rb[H_2C_3N_3O_3]\cdot H_2O$-II (**2**) [(b) Rb1 and (d) Rb2] with atoms shown as thermal anisotropic ellipsoids (50 %).

$Rb[H_2C_3N_3O_3]\cdot H_2O$-II (**2**) also crystallizes in a new structure type adopting space group $P\bar{1}$ (no. 2), the unit cell is depicted in Figure 1b. The crystal structure is very similar to that of $Rb[H_2C_3N_3O_3]\cdot H_2O$-I (**1**), thus only the differences are discussed in detail. In contrast to **1**, adjacent isocyanurate anions are tilted towards each other (dihedral angle: 4.3°, Figure S1a), forming a slightly undulated ribbon. These ribbons are tilted approx. 82° towards the Rb^+-H_2O layers and are stacked alternately leading to an AABB layer sequence in **2**, in contrast to the AAAA sequence **1** (Figure S1b, Supporting Information). This yields larger voids for the Rb^+-cations and therefore larger coordination numbers. A fourth deprotonated nitrogen atom enters the coordination sphere of Rb1 (Figure S1c, Supporting Information) and a distorted tetracapped trigonal prism (CN = 10) is achieved. Hence, all deprotonated nitrogen atoms coordinate two Rb^+ cations. Rb2 is surrounded by six carbonyl oxygen atoms and three water molecules, now forming a distorted monocapped tetragonal antiprism (CN = 9).

This environment may alternatively be described as a trigonal prism capped on two tetragonal and one trigonal face, in order to show the close relationship to the Rb2 in **1**, where only tetragonal faces are capped. The interatomic distances between Rb and the surrounding atoms correspond on average (3.02 Å and 3.10 Å for CN = 9 and CN = 10, respectively) well with the sum of the respective ionic radii (3.00 Å and 3.07 Å). All this causes a less dense packing, resulting in a density of 2.33 g·cm^{-3} for **2**, compared to 2.35 g·cm^{-3} for **1**. We did not perform further investigations regarding other properties on **1** and **2** due to impurities in all synthesized samples at the current stage of our research (see Experimental Section).

$Rb_3[H_2C_3N_3O_3]_3[H_3C_3N_3O_3]\cdot 4H_2O$ (4)

The crystal structure of **4** was already reported by *Nichols* et al.[10] and we would like to refer the reader to their publication for a detailed discussion of the structure. We confirmed their findings in several single-crystal XRD studies. As we were able to synthesize phase pure samples, we also shed light upon the spectroscopic and thermal properties of **4**. The X-ray powder diffraction pattern (Figure S2, Supporting Information) reveals a strongly preferred orientation of the crystallites towards the (2 1 2)-face in accordance with plate-like crystallites on a flat sample holder. The FT-IR spectrum is shown in Figure 5, the frequencies of all peaks are tabulated in Table S1 (Supporting Information) and assigned to vibrational modes to the best of the authors' knowledge, as well as compared to the frequencies of $Cs[H_2C_3N_3O_3]\cdot 0.5H_2O$ (**3**), cyanuric acid and to typical frequencies found in literature for similar compounds.

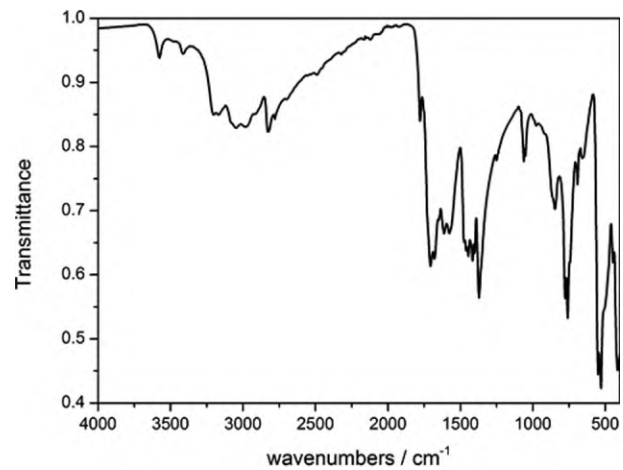

Figure 5. FT-IR spectrum of $Rb_3[H_2C_3N_3O_3]_3[H_3C_3N_3O_3]\cdot 4H_2O$ (**4**).

A careful comparison with the spectrum of **3** and those of similar chemical species[7,20] shows a close matching of most of the frequencies. To explain the additional peaks, we recorded a FT-IR spectrum of cyanuric acid (98 %, Merck) for comparison (Table S1, Supporting Information). Thus it is possible to explain all remaining vibrational modes by fully pro-

tonated $[H_3C_3N_3O_3]$ moieties and thereby prove their presence.[10] The UV/Vis spectrum (Figure S3, Supporting Information) shows a distinct absorption edge at about 240 nm, presumably corresponding to the bandgap of **4** in good accordance with that at 220 nm determined for cyanuric acid.[2,21]

We also studied the thermal decomposition behavior evaluating the potential use as a precursor to nitridocarbonates; thermogravimetric analyses were performed on **4**. The thermogravimetry plot (Figure 6, black line) exhibits two main steps of mass loss, very similar to that of **3** (Figure 10). The small step between 70 °C and 205 °C (Δm = 8.5 %) corresponds very well with the calculated value (8.6 %) for the loss of four equivalents of crystal water molecules per formula unit. The second, more complex and larger step between 270 °C and 400 °C consists actually of two overlapping sub-steps and an intense overlaying thermal effect (explained below) between 360 °C and 390 °C. This larger step (41.7 %) might correspond to the decomposition of cyanuric acid to cyanic acid and the decomposition of $Rb[H_2C_3N_3O_3]$ to Rb[OCN] and cyanic acid, which are both reported to occur in this temperature ranges.[9] Since these processes would result in a total mass loss of 45.9 %, such a simple decomposition process can be ruled out. Apparently, more complex reactions take place, well known to occur easily for molecular compounds and cyanate melts.[22,23] From the plot of the temperature vs. time (Figure 6, red curve) it can be deduced that this effect occurs due to an endothermic process. Since its thermal position coincides very well with the monomerization temperature of a $[C_3N_3O_3]^{3-}$ anion yielding three $[OCN]^-$ anions as reported for rubidium isocyanurate (360 °C[9]) as well as for the monomerization of cyanuric acid, we conclude this effect to be caused by such monomerization processes. A subsequent, more detailed study of the thermal properties of alkali isocyanurates is currently in progress.

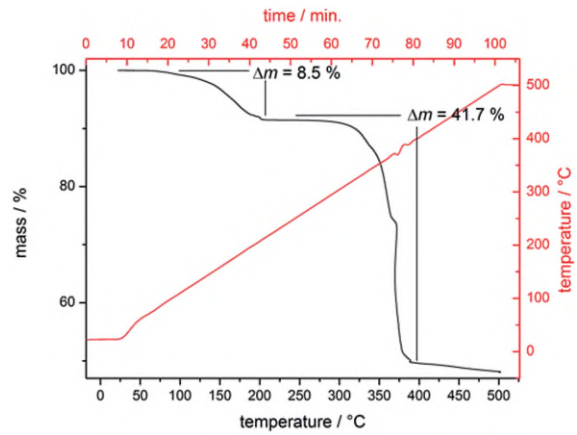

Figure 6. Thermogram of $Rb_3[H_2C_3N_3O_3]_3[H_3C_3N_3O_3]\cdot 4H_2O$ (**4**) shown in black (left *y* axis, bottom *x* axis) and the temperature as a function of time shown in red (right *y* axis, top *x* axis).

$Cs[H_2C_3N_3O_3]\cdot 0.5H_2O$ (3)

Compound **3** crystallizes in its own structure type in the space group $P2_1/m$ (no. 11) and shows structural motifs similar to $Rb[H_2C_3N_3O_3]\cdot H_2O$ (**1** and **2**). The unit cell is depicted in Figure 7. The crystal structure exhibits dibasic isocyanurate anions $[H_2O_3C_3N_3]^-$ with typical bond lengths and angles (Figure 8a), interconnected by strong hydrogen bonds[19] to form infinite ribbons of isocyanurate anions (Figure 8b). Adjacent isocyanurate anions are tilted by 5.6° and 9.8° resulting in slightly undulated ribbons. This ribbon motif is frequently encountered and present in all alkali[10–12] and 3d transition metal-isocyanurate[15–17] structures hitherto found. These ribbons are stacked along [100] to form isocyanurate layers (Figure 8c) similar to those in **1** and **2**; here, the isocyanurate anions of alternate layers are tilted towards each other by approx. 50°.

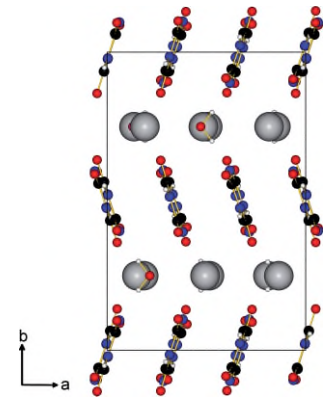

Figure 7. The unit cell of $Cs[H_2C_3N_3O_3]\cdot 0.5H_2O$ (**3**) viewed along [001]. (Cs: grey spheres, C: black spheres, N: blue spheres, O: red spheres and H: white spheres, covalent bonds: yellow sticks).

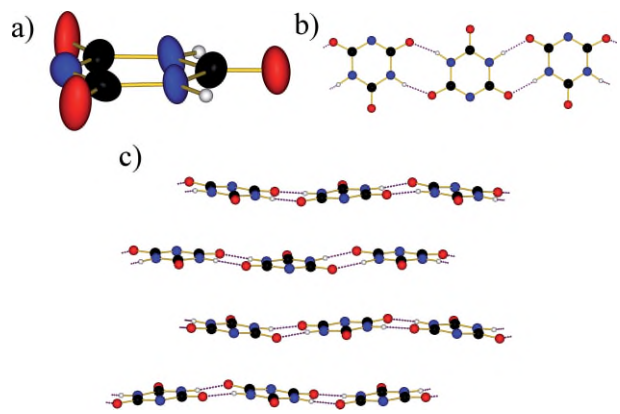

Figure 8. Ball-and-stick-model of the $[H_2C_3N_3O_3]^-$ anion in $Cs[H_2C_3N_3O_3]\cdot 0.5H_2O$ (**3**). (a) Atoms shown as thermal ellipsoids (50 %). (b) Isocyanurate-ribbon depicted from top. (c) Layers resulting from stacked isocyanurate ribbons.

The isocyanurate layers are separated by layers of Cs^+ cations and water molecules. The Cs^+ cations are distributed over six independent crystallographic sites (Figure S4, Supporting Information). Cs1, Cs2, and Cs3 are surrounded by six carbonyl oxygen atoms and two water molecules forming distorted tetragonal antiprisms (CN = 8). Cs4, Cs5, and Cs6 are surrounded by six carbonyl oxygen atoms, two deprotonated nitrogen atoms, and two water molecules forming distorted centaur polyhedra (CN = 10).[24] The interatomic distances between Cs and the surrounding atoms correspond on average

(3.20 Å and 3.27 Å for CN = 8 and CN = 10, respectively) well with the sum of the respective ionic radii (3.12 Å and 3.21 Å). According to the X-ray powder diffraction pattern (Figure S5, Supporting Information), we were able to synthesize phase pure samples of **3**.

The FT-IR spectrum of **3** is shown in Figure 9. The frequencies of all peaks are listed in Table S1 (Supporting Information) and assigned to vibrational modes to the best of our knowledge, as well as compared to the frequencies of **4**, cyanuric acid and to typical frequencies found in literature for similar compounds. The frequencies of all observed bands correspond well with the expected frequencies of the assumed chemical species.[9,20] The UV/Vis spectrum (Figure S11, Supporting Information) shows a distinct absorption edge at about 240 nm, presumably corresponding to the bandgap of **3** in good accordance with that at 220 nm determined for cyanuric acid.[2,21]

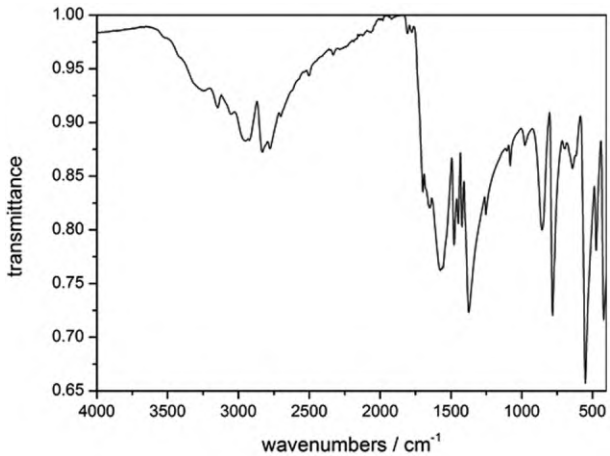

Figure 9. FT-IR spectrum of $Cs[H_2C_3N_3O_3]\cdot 0.5H_2O$ (**3**).

The thermogravimetry plot (Figure 10) exhibits two main steps of mass loss, very similar to that of **4** shown in Figure 8. The small step between 70 °C and 205 °C (Δm = 3.7 %) corresponds well with the calculated value (3.3 %) for the loss of 0.5 equiv. of crystal water per formula unit.

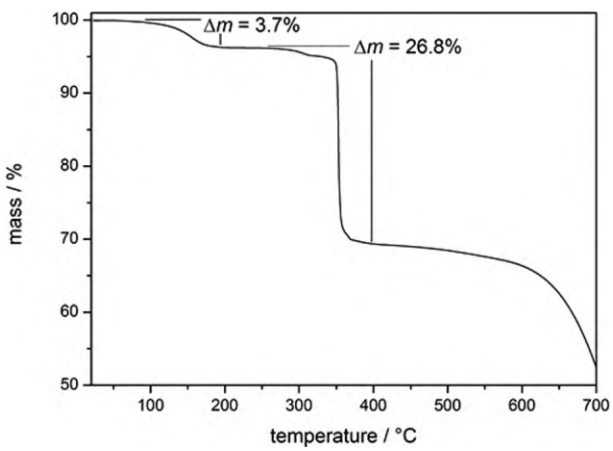

Figure 10. Thermogram of $Cs[H_2C_3N_3O_3]\cdot 0.5H_2O$ (**3**).

The higher experimental value can be explained by additional humidity adsorbed on the crystallites' surface due to the slight hygroscopicity of the compound. The second, more complex and larger step between 270 °C and 400 °C consists actually of two strongly overlapping sub-steps. This larger step (26.8 %) is described in literature as corresponding to the decomposition of $Cs[H_2C_3N_3O_3]$ to Cs[OCN] and cyanic acid.[9] Since these processes would result in a total mass loss of 31.9 %, such a simple decomposition process can be ruled out with the same arguments mentioned on **4**. A subsequent, more detailed study on the thermal properties of alkali isocyanurates is currently in progress.

$Sr[H_2C_3N_3O_3]_2\cdot 4H_2O$ (7)

Compound **7** crystallizes in its own structure type in space group $P2_1/c$ (no. 14), unfortunately the reflection conditions for the glide plane show weak but significant violations. An alternative twin refinement in $P2_1$ (no. 4) yielded better residuals wR_2 (0.071) and R_1 (0.037) with BASF = 0.53(1); all structural parameters were of similar quality, though. Therefore, a description in the higher symmetric space group is actually preferred – a final decision might be subject of a SHG experiment yet to come. The crystal structure is plotted in Figure 11a and exhibits dibasic isocyanurate anions $[HO_3C_3N_3]^-$ with typical bond lengths (1.34–1.38 Å for C–N and 1.25–1.28 Å for C–O) and angles (Figure 12a). These anions are interconnected by strong hydrogen bonds[19] via N–H···O=C and N–H···N moieties to form slightly corrugated, infinite ribbons along [210] (Figure 12b). Though this ribbon motif is often encountered in metal isocyanurate chemistry.[10–17], its connectivity pattern is to the best of our knowledge unprecedented as N–H···N hydrogen bonds have hitherto not been described for isocyanurate ribbons. The ribbons are stacked along [100] and thus form isocyanurate layers (Figure 12c). The voids between the isocyanurate layers host Sr^{2+} cations and water molecules. These connect neighboring isocyanurate layers via hydrogen bonds towards most of the deprotonated nitrogen atoms and act as hydrogen bond acceptors towards some protonated nitrogen atoms.

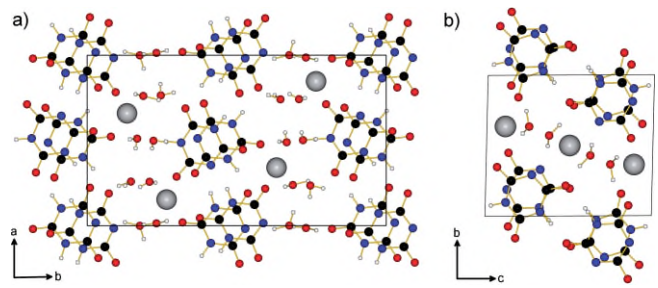

Figure 11. The unit cell of (a) $Sr[H_2C_3N_3O_3]_2\cdot 4H_2O$ (**7**) along [001] and (b) $Ba_3[H_2C_3N_3O_3]_2[H_2C_3N_3O_3]_2\cdot 4H_2O$ (**11**) along [100] (Ba/Sr: grey spheres, C: black spheres, N: blue spheres, O: red spheres and H: white spheres, covalent bonds: yellow sticks).

The Sr^{2+} cations are located on two crystallographically different sites, Sr1 and Sr2 (Figure S6, Supporting Information); both are coordinated by four H_2O molecules and four carbonyl

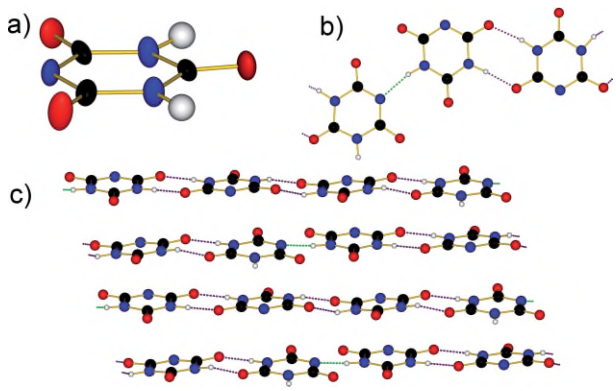

Figure 12. Ball-and-stick-model of the $[H_2C_3N_3O_3]^-$ anion in $Sr[H_2C_3N_3O_3]_2{\cdot}4H_2O$ (**7**) (hydrogen bonds N–H···O: broken violet lines, hydrogen bonds N–H···N: broken green lines); (a) atoms shown as thermal anisotropic ellipsoids (50%); (b) isocyanurate-ribbon depicted from top; (c) layers resulting from stacked isocyanurate ribbons.

oxygen atoms forming a slightly distorted square antiprism (CN = 8). The interatomic distances between Sr and the surrounding atoms correspond on average (2.60 Å) well with the sum of the ionic radii (2.64 Å).

$Ba_3[H_2C_3N_3O_3]_2[HC_3N_3O_3]_2{\cdot}4H_2O$ (11)

Compound **11** crystallizes in its own structure type in space group $P\bar{1}$ (no. 2). The crystal structure, shown in Figure 11b, comprises monobasic isocyanurate anions $[H_2O_3C_3N_3]^-$ as well as dibasic isocyanurate anions $[HO_3C_3N_3]^{2-}$ with typical bond lengths (1.34–1.39 Å for C–N and 1.21–1.28 Å for C–O) and angles (Figure 13a). These anions form dimers by strong hydrogen bonds[19] according to N–H···O=C moieties of two neighboring anions.

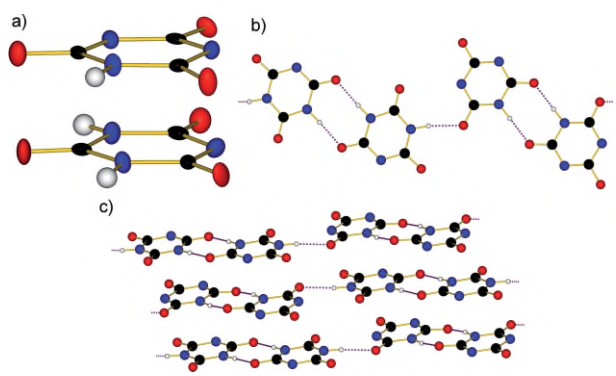

Figure 13. Ball-and-stick-model of the $[H_2C_3N_3O_3]^-$- and the $[HC_3N_3O_3]^{2-}$ anion in $Ba_3[H_2C_3N_3O_3]_2[H_2C_3N_3O_3]_2{\cdot}4H_2O$ (**11**) (hydrogen bonds: broken violet lines); (a) atoms shown as thermal anisotropic ellipsoids (50%); (b) isocyanurate-ribbon depicted from top; (c) layers resulting from stacked isocyanurate ribbons.

The dimers are further connected via a single hydrogen bond to two adjacent dimers (Figure 13b), resulting in strongly corrugated isocyanurate ribbons along [210]. Again, this represents an unprecedented type of the generally often encountered isocyanurate ribbons,[10–17] as it contains monobasic as well as dibasic isocyanurate anions. The resulting ribbons are stacked along [101] (Figure 13c). Between adjacent layers the Ba^{2+} cations and H_2O molecules are found. The water molecules connect neighboring isocyanurate layers via hydrogen bonds towards the deprotonated nitrogen atoms. Ba^{2+} cations are distributed over two sites (Figure S7, Supporting Information); Ba1 is coordinated by two water molecules, six carbonyl oxygen atoms and a single deprotonated nitrogen atom forming a distorted gyroelongated square pyramid (CN = 9), while Ba2 is coordinated by four water molecules, four carbonyl oxygen atoms, and four deprotonated nitrogen atoms (CN = 12).

The coordination polyhedron of Ba2 can be either described as heavily distorted icosahedron or as tetragonal prism spanned by carbonyl oxygen and deprotonated nitrogen atoms tetracapped by water molecules above the elongated faces. The interatomic distances between Ba and the surrounding atoms correspond on average (2.82 Å and 3.00 Å for CN = 9 and CN = 12, respectively) well with the sum of the ionic radii (2.85 Å and 2.99 Å).

$Ca[HC_3N_3O_3]{\cdot}3.5H_2O$ (6)

Compound **6** crystallizes in its own structure type in space group $P2_1/c$ (no. 14). The crystal structure (Figure 14a) exhibits dibasic isocyanurate anions $[HO_3C_3N_3]^{2-}$ with typical bond lengths (1.34–1.38 Å for C–N and 1.25–1.28 Å for C–O) and angles (Figure 15a). These anions form dimers via strong hydrogen bonds[19] between the protonated nitrogen atoms and a carbonyl oxygen atom of a neighboring anion (Figure 15b). The dimers are aligned parallel to (101) and stacked to columns (Figure 15c) with rhomboidal cross section along [100]. The columns form two interpenetrating primitive tetragonal rod packings differing in their respective dimer-alignment [broader face of the rod parallel to (011) and (01–1), respectively], as indicated in Figure 15d. Intersecting, corrugated layers of H_2O molecules and Ca^{2+} cations are situated between these rods. The water molecules connect neighboring isocyanurate columns via hydrogen bonds. The Ca^{2+} cations are located on two sites (Figure S8, Supporting Information); Ca1 is coordinated by six water molecules and two carbonyl oxygen atoms forming a distorted cube (CN = 8), Ca2 is coordinated

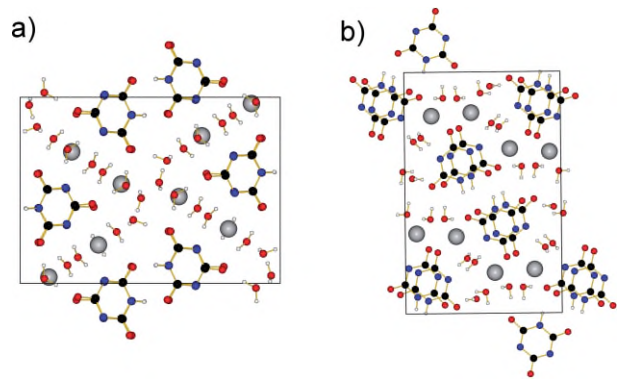

Figure 14. The unit cell of (a) $Ca[HC_3N_3O_3]{\cdot}3.5H_2O$ (**6**) along [001] and (b) $Sr[HC_3N_3O_3]{\cdot}3H_2O$ (**8**) along [100] (Ca/Sr: grey spheres, C: black spheres, N: blue spheres, O: red spheres and H: white spheres, covalent bonds: yellow sticks).

by five water molecules, two carbonyl oxygen atoms and two deprotonated nitrogen atoms forming a distorted elongated square-pyramid (CN = 9). The interatomic distances between Ca and the surrounding atoms correspond on average (2.50 Å and 2.57 Å for CN = 8 and CN = 9, respectively) very well with the sum of the ionic radii (2.50 Å for CN = 8 and 2.56 Å for CN = 9).

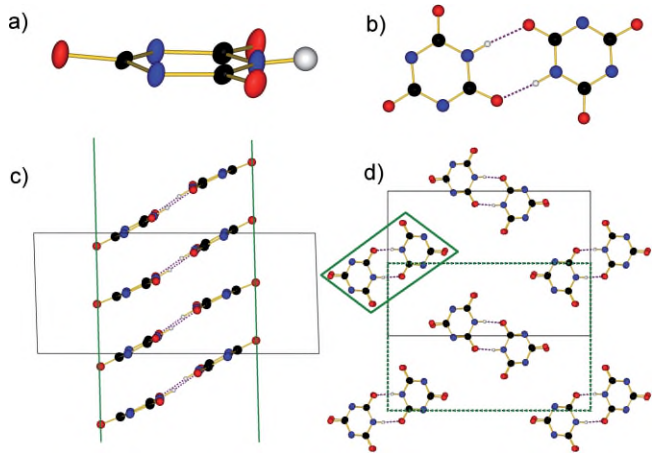

Figure 15. Ball-and-stick model of the $[HC_3N_3O_3]^{2-}$ anion in $Ca[HC_3N_3O_3]\cdot 3.5H_2O$ (**6**) (hydrogen bonds: broken violet lines); (a) atoms shown as thermal anisotropic ellipsoids (50 %).; (b) isocyanurate dimer depicted from top; (c) column resulting from stacked isocyanurate-dimers; (d) rod packing of columns (solid green lines indicate column faces, broken green lines indicates packing scheme).

Sr[HC$_3$N$_3$O$_3$]·3H$_2$O (8)

Compound **8** crystallizes in its own structure type in the space group $P2_1/c$ (no. 14). The crystal structure shown in Figure 14b is in most aspects similar to that of $Ca[HC_3N_3O_3]\cdot 3.5H_2O$ (**6**), also featuring dibasic isocyanurate anions $[HO_3C_3N_3]^{2-}$ (Figure 16a) with typical bond lengths (1.34–1.38 Å for C–N and 1.2–1.28 Å for C–O) and angles, which form dimers (Figure 16b). The dimers are aligned parallel to (110) and stacked to columns with rhomboidal cross section along [100] (Figure 16c), arranged in two interpenetrating primitive tetragonal rod packings analogously to $Ca[HC_3N_3O_3]\cdot 3.5H_2O$ (Figure 16d). H_2O molecules (connecting neighboring columns by hydrogen bonds) and Sr^{2+} cations (two crystallographic sites) are found in the voids between the columns. Slight differences to $Ca[HC_3N_3O_3]\cdot 3.5H_2O$ are found for the coordination environment of the cations, as seen in Figure S9 (Supporting Information). Sr1 is coordinated by four water molecules and four carbonyl oxygen atoms forming a distorted tetragonal antiprism (CN = 8) and Sr2 is coordinated by six water molecules, two carbonyl oxygen atoms and one deprotonated nitrogen atom forming a distorted gyroelongated square-pyramid (CN = 9). The interatomic distances between Sr and the surrounding atoms correspond on average (2.69 Å and 2.68 Å for CN = 8 and CN = 9, respectively) well with the sum of the ionic radii (2.64 Å and 2.69 Å).

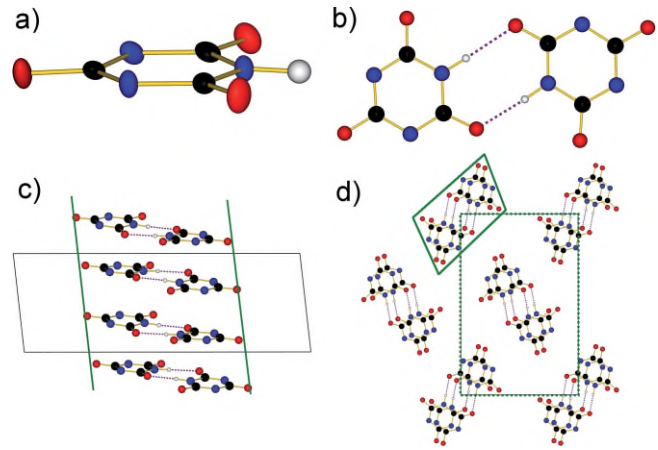

Figure 16. Ball-and-stick model of the $[HC_3N_3O_3]^{2-}$ anion in $Sr[HC_3N_3O_3]\cdot 3H_2O$ (**8**) (hydrogen bonds: broken violet lines); (a) atoms shown as thermal anisotropic ellipsoids (50 %); (b) isocyanurate-dimer depicted from top; (c) column resulting from stacked isocyanurate dimers; (d) rod packing of columns (solid green lines indicate column faces, broken green line indicates packing scheme).

Sr[HC$_3$N$_3$O$_3$]·2H$_2$O (10)

Compound **10** crystallizes in its own structure type in space group *Ima*2 (no. 46), the unit cell is depicted in Figure 17a. The crystal structure comprises dibasic isocyanurate anions $[HO_3C_3N_3]^{2-}$ (Figure 18a) with typical bond lengths (1.33–1.38 Å for C–N and 1.26–1.27 Å for C–O) and angles. These anions form chains along [010] by single hydrogen bonds between the protonated nitrogen atom and a carbonyl group of a neighboring anion (Figure 18b), which are hitherto unknown in isocyanurate chemistry. The chains are stacked antiparallel face-centred along [001] and thus also form a new type of isocyanurate layers (Figure 18c). The voids between the isocyanurate layers host Sr^{2+} cations and H_2O molecules. The water molecules connect the stacked isocyanurate chains within a layer via hydrogen bonds.

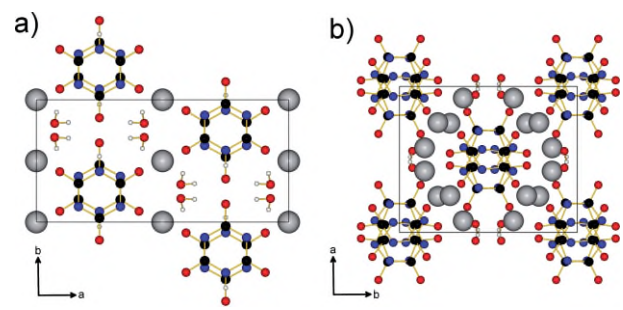

Figure 17. The unit cell of (a) $Sr[HC_3N_3O_3]\cdot 2H_2O$ (**10**) along [001] and (b) $Sr_2[C_3N_3O_3]OH$ (**9**) along [100] (Sr: grey spheres, C: black spheres, N: blue spheres, O: red spheres and H: white spheres, covalent bonds: yellow sticks).

The Sr^{2+} cations are coordinated by four water molecules, two carbonyl oxygen atoms and two deprotonated nitrogen atoms forming a distorted square antiprism (CN = 8, Figure S10, Supporting Information). The interatomic distances between Sr and the surrounding atoms correspond on average (2.68 Å) well with the sum of the ionic radii (2.64 Å).

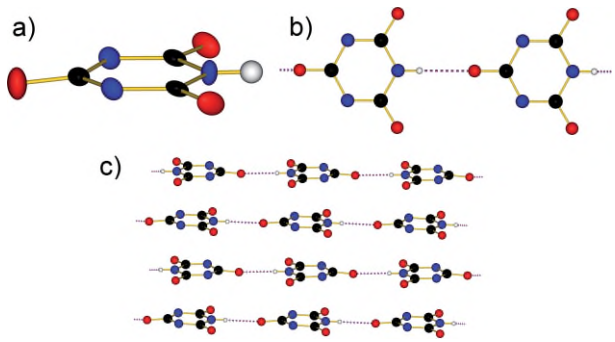

Figure 18. Ball-and-stick model of the $[HC_3N_3O_3]^{2-}$ anion in $Sr[HC_3N_3O_3]\cdot 2H_2O$ (**10**) (hydrogen bonds: broken violet line); (a) atoms shown as thermal anisotropic ellipsoids (50 %); (b) isocyanurate chain depicted from top; (c) layers resulting from stacked isocyanurate chains.

$Sr_2[C_3N_3O_3]OH$ (9)

Compound **9** crystallizes in its own structure type in space group *C*2/*c* (no. 15). The crystal structure (Figure 17b) exhibits tribasic cyanurate anions $[O_3C_3N_3]^{3-}$ (Figure 19a) with typical bond lengths (1.35–1.37 Å for C–N and 1.27–1.30 Å for C–O) and angles. These cyanurate anions are aligned parallel to (10 0 3) and stacked alternately antiparallel face-centred and antiparallel offset along [001] (Figure 19b) to form columns with a distorted hexagonal cross section, arranged in a face-centred tetragonal rod packing (Figure 19c). OH^- anions and Sr^{2+} cations are located in the voids between the columns. Each hydroxide anion acts as hydrogen-bond donor both towards a neighboring carbonyl oxygen atom as well as a nitrogen atom belonging to a single $[O_3C_3N_3]^{3-}$ anion.

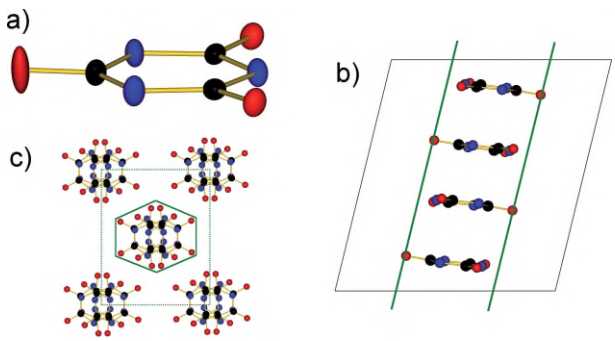

Figure 19. Ball-and-stick model of the $[C_3N_3O_3]^{2-}$ anion in $Sr_2[C_3N_3O_3]OH$ (**9**); (a) atoms shown as thermal anisotropic ellipsoids (50 %). (b) Column resulting from stacked cyanurate anions; (c) rod packing of columns (solid green lines indicate column faces).

The Sr^{2+} cations occupy two different sites (Figure 20); Sr1 is coordinated by two hydroxide anions, for carbonyl oxygen atoms and two nitrogen atoms forming a distorted tetragonal antiprism (CN = 8), while Sr2 is coordinated by a single hydroxide anion, for carbonyl oxygen atoms and three nitrogen atoms forming a quite unusual distorted prismatoid spanned by a trigon and a pentagon (CN = 8). The interatomic distances between Sr and the surrounding atoms correspond on average (2.67 Å) well with the sum of the ionic radii (2.64 Å).

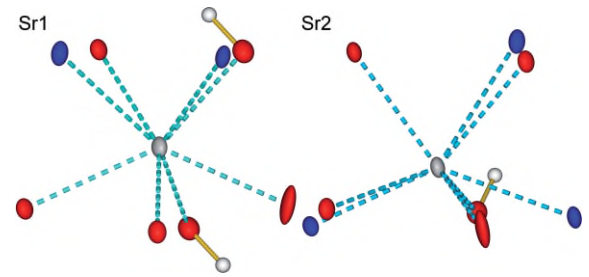

Figure 20. Coordination environment of the Sr atoms in $Sr_2[C_3N_3O_3]OH$ (**9**) with atoms shown as thermal anisotropic ellipsoids (50 %).

Further Characterization of $Sr[HC_3N_3O_3]\cdot 2H_2O$ (10)

As obtaining phase pure samples required elaborate control of the pH and the CO_2 concentration during crystallization as well as of the humidity during the subsequent handling, we limited further characterization to $Sr[HC_3N_3O_3]\cdot 2H_2O$ as the most promising precursor for $Sr_3[C_3N_3O_3]_2$, a prominent NLO material,[2] and Sr[NCN], a host structure for orange luminescence via Eu^{2+} doping[25,26] as well as a possible starting material for carbothermal reduction synthesis of nitride phosphors.[27,28] After proving phase purity by powder X-ray diffraction (Figure S1, Supporting Information), we exemplarily determined the vibrational, optical and thermal properties of $Sr[HC_3N_3O_3]\cdot 2H_2O$.

The frequencies (Table S2, Supporting Information) obtained from the FT-IR spectrum (Figure 21) were assigned to vibrational modes to the best of the authors' knowledge and correspond well to the typical frequencies found in literature for such compounds. The UV/Vis spectrum (Figure S13, Supporting Information) shows an absorption edge centred at 216 nm, which can be understood as the bandgap of $Sr[HC_3N_3O_3]\cdot 2H_2O$. To study the thermal decomposition, especially in consideration of the potential utilization as a precursor compound, we performed a thermogravimetric study of

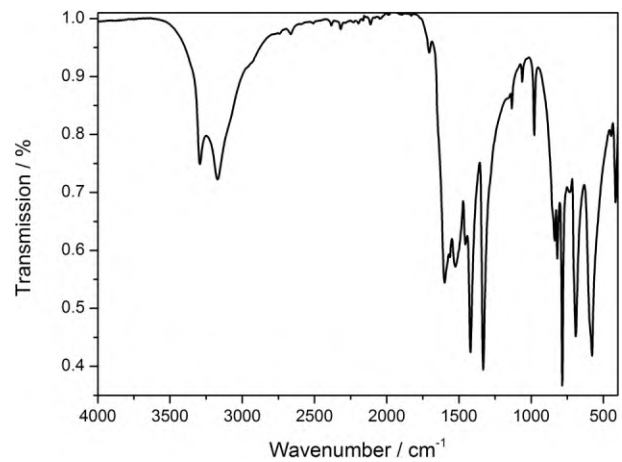

Figure 21. FT-IR spectrum of $Sr[HC_3N_3O_3]\cdot 2H_2O$ (**10**).

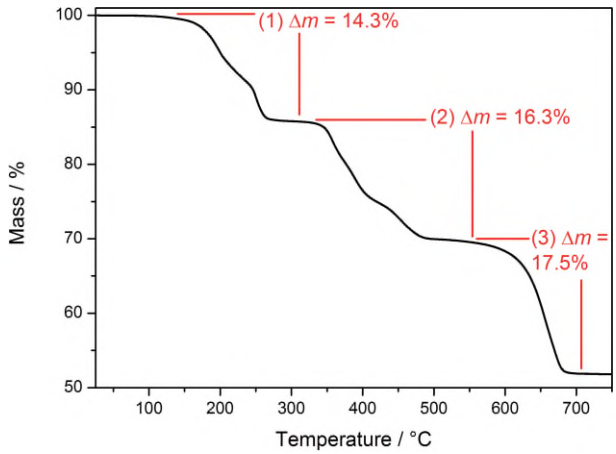

Figure 22. Thermogram of $Sr[HC_3N_3O_3]\cdot 2H_2O$ (**10**).

$Sr[HC_3N_3O_3]\cdot 2H_2O$. The thermogram (Figure 22) shows three main steps of mass loss; the first consists of at least two and the second of at least three overlapping processes, summarized in the proposed reaction scheme below:

(I) $Sr[HC_3N_3O_3]\cdot 2H_2O \rightarrow Sr[HC_3N_3O_3] + 2H_2O$ (Δm = 14.4 %)

(II) $3Sr[HC_3N_3O_3] \rightarrow Sr_3[C_3N_3O_3]_2 + 3HNCO$ (Δm = 17.1 %)

(III) $Sr_3[C_3N_3O_3]_2 \rightarrow 3Sr[NCN] + 3CO_2$ (Δm = 17.6 %)

In order to validate these proposed reactions, $Sr[HC_3N_3O_3]\cdot 2H_2O$ was heated in a furnace to 450 °C and 650 °C, respectively, and the products were found to be $Sr_3[C_3N_3O_3]_2$ and β-Sr[NCN] (Figures S14 and S15, Supporting Information). Several more detailed studies on the reaction mechanism for thermal decomposition of alkaline-earth isocyanurates are summarized in reference[9] and were found to be in complete agreement with or findings.

Conclusions

Careful crystallization from aqueous solution proved to be an easy and powerful method for obtaining high-quality crystals of metal isocyanurate hydrates suitable for single-crystal XRD. By this approach we were able to significantly expand the hitherto limited structural knowledge for the alkali and alkaline-earth isocyanurate hydrates. Crystallization conditions for the several degrees of deprotonation of cyanuric acid were confirmed to be mostly dependant on the solvent's pH, and with $Sr_2[C_3N_3O_3]OH$ we obtained for the first time a tribasic metal cyanurate by crystallization from aqueous solution. Several novel topologies of hydrogen bonded isocyanurate ribbons were found – like columns of dimers, chains of singly bonded isocyanurate units, or ribbons featuring N–H···N bonds. IR spectroscopy is an excellent auxiliary tool for the differentiation between several cyanuric acid species varying in their respective degree of deprotonation, despite the fact that they crystallize simultaneously.

Air- and moisture-resistant $Sr[HC_3N_3O_3]\cdot 2H_2O$ could be prepared as a phase pure sample in a very simple and straightforward synthesis from cheap and common reagents. Thermal studies proved that it is an excellent precursor material for $Sr_3[C_3N_3O_3]_2$ and Sr[NCN], both obviously interesting as optical materials. Preparation and handling of phase pure samples remains a challenge for several alkali and alkaline-earth isocyanurates. A phase pure synthesis for each of the two modifications of $Rb[H_2C_3N_3O_3]\cdot H_2O$ remains a future challenge and illustrates some of the obstacles that have to be overcome: besides an exact control of a vast number of parameters (including temperature, pH, concentration, stoichiometry, reaction atmosphere) during the whole crystallization process, polymorphism caused by only slight variations of the stacking sequence results in similar densities pointing towards similar stabilities according to Ostwald's rule.[32] Thermal decomposition of metal isocyanurates seems to be less straight forward in many cases than believed throughout the literature[9] and remains to be fully elucidated and understood.

Experimental Section

Synthesis: All chemicals were used without further purification and were handled in air. While the synthesis for $Cs[H_2C_3N_3O_3]\cdot 0.5H_2O$ (**3**) yielded a phase pure product, the same approach for an analogous Rb compound yielded a mixture of $Rb[H_2C_3N_3O_3]\cdot H_2O$-I (**1**), $Rb[H_2C_3N_3O_3]\cdot H_2O$-II (**2**), and $Rb_3[H_2C_3N_3O_3]_3[H_3C_3N_3O_3]\cdot 4H_2O$ (**4**). All alkali isocyanurates were synthesized via acid-base reaction in aqueous solution followed by slow evaporation to dryness. All three crystals for single-crystal XRD of these Rb compounds were picked from the same sample. $Sr[H_2C_3N_3O_3]_2\cdot 4H_2O$ (**7**), $Ba_3[H_2C_3N_3O_3]_2[HC_3N_3O_3]_2\cdot 4H_2O$ (**11**), $Ca[HC_3N_3O_3]\cdot 3.5H_2O$ (**6**), and $Sr[HC_3N_3O_3]\cdot 3H_2O$ (**8**) were synthesized via salt metathesis in a U-tube, $Sr_2[C_3N_3O_3]OH$ (**9**) was synthesized hydrothermally and $Sr[HC_3N_3O_3]\cdot 2H_2O$ (**10**) was obtained via dehydration of $Sr[HC_3N_3O_3]\cdot 3H_2O$.

$Rb[H_2C_3N_3O_3]\cdot H_2O$-I (1) and $Rb[H_2C_3N_3O_3]\cdot H_2O$-II (2): Rb_2CO_3 (115.5 mg, 0.5 mmol, 99 %, Alfa Aesar) was dissolved in 40 mL H_2O (deionized) in a beaker. Cyanuric acid (129.1 mg, 1 mmol, 98 %, Merck) was added and the resulting suspension was gently heated under magnetic stirring on a hot plate (ca. 80 °C). As soon as a clear solution was obtained, the beaker was removed from the hot plate and the solution was pored into a petri dish. The water was evaporated overnight at about 30 °C. Colorless crystals in form of cubic blocks ($Rb_3[H_2C_3N_3O_3]_3[H_3C_3N_3O_3]\cdot 4H_2O$) and thick, rhombohedral plates ($Rb[H_2C_3N_3O_3]\cdot H_2O$-I and $Rb[H_2C_3N_3O_3]\cdot H_2O$-II) were obtained.

$Rb_3[H_2C_3N_3O_3]_3[H_3C_3N_3O_3]\cdot 4H_2O$ (4): Rb_2CO_3 (115.5 mg, 0.5 mmol, 99 %, Alfa Aesar) was dissolved in 40 mL H_2O (deionized) in a beaker. Cyanuric acid (172.1 mg, 1.33 mmol, 98 %, Merck) was added and the resulting suspension was gently heated under magnetic stirring on a hot plate (ca. 80 °C). As soon as a clear solution was obtained, the beaker was removed from the hot plate and the solution was poured into a petri dish. The water was evaporated overnight at about 30 °C. Colorless, cubic crystals (which easily break to form very thin plates) were obtained with a yield of 96 %.

$Cs[H_2C_3N_3O_3]\cdot 0.5H_2O$ (3): Cs_2CO_3 (162.9 mg, 0.5 mmol, 99.9 %, SIGMA-ALDRICH) was dissolved in 40 mL H_2O (deionized) in a beaker. Cyanuric acid (129.1 mg, 1 mmol, 98 %, Merck) was added and the resulting suspension was gently heated under magnetic stirring on a hot plate (ca. 80 °C). As soon as a clear solution was obtained, the beaker was removed from the hot plate and the solution was poured into a petri dish. The water was evaporated overnight at about 30 °C. Slightly hygroscopic, colorless crystals in form of thin, tetragonal plates and aggregates thereof were obtained with a yield of 98 %.

U-tube Syntheses: For the syntheses of $Sr[H_2C_3N_3O_3]_2\cdot 4H_2O$ (**7**), $Ba_3[H_2C_3N_3O_3]_2[HC_3N_3O_3]_2\cdot 4H_2O$ (**11**), $Ca[HC_3N_3O_3]\cdot 3.5H_2O$ (**6**), and $Sr[HC_3N_3O_3]\cdot 3H_2O$ (**8**) the approach described hereafter was adopted. In a typical experiment, two freshly prepared aqueous solution (5–15 mL) of an alkaline earth chloride and sodium cyanurate (made from sodium hydroxide and cyanuric acid in a molar ratio of 3:1), respectively, were used as starting materials. The reaction was performed as a salt metathesis via slow interdiffusion of these reagents through an isoosmotic NaCl solution in a U-tube. Therefore, the U-tube was first filled with the NaCl solution and cooled with ice water. Meanwhile, the two reactant solutions are heated to about 80 °C. Subsequently, a glass rod is placed at the solution-air interface of the NaCl solution and each of the two reactant solutions is poured very slowly on top of the NaCl solution in order to avoid mixing as far as practible on the respective side of the U-tube. In the course of 1–4 d, colorless crystals up to a few centimetres long and suitable for single-crystal XRD appeared at the bottom of the U-tube. A series of photos of the crystallization of **8** was recorded and rendered into a video (available as Supporting Information). Masses, volumes, purity, and supplier of the chemicals employed during these syntheses are listed in Table 1.

$Sr_2[C_3N_3O_3]OH$ (9): Cyanuric acid (1 mmol, 129.1 mg, Merck, 98 %), NaOH (10 mmol, 400 mg, VWR Chemicals, 99 %) and 2 mL demineralized H_2O were placed into a a PTFE digestion vessel (10 mL, BOLA). The vessel was sealed, heated at 120 °C in a preheated compartment dryer for 15 min and subsequently allowed to cool until luke warm. $SrCl_2\cdot 6H_2O$ (1.5 mmol, 400.0 mg, Aldrich, 99 %) was dissolved in 2 mL demineralized H_2O and poured into the digestion vessel, which was closed immediately afterwards. The vessel was placed again in the preheated compartment dryer (120 °C) and left there for 17 h. Afterwards, it was allowed to cool to room temperature. Colorless crystals suitable for single-crystal xrd were directly picked from the obtained dispersion.

$Sr[HC_3N_3O_3]\cdot 2H_2O$ (10): $Sr[HC_3N_3O_3]\cdot 3H_2O$ was obtained via slow interdiffusion metathesis as described above was filtered off from the mother liquor with filter paper and funnel, washed with demineralized water, ethanol and acetone and finally the filter paper was placed in an uncovered petri dish and allowed to dry overnight at about 40 °C in air. A phase pure sample of $Sr[HC_3N_3O_3]\cdot 2H_2O$ was obtained, which contained crystals suitable for single-crystal xrd.

X-ray Structure Determination: Suited single crystals were selected for single-crystal XRD under a polarizing microscope. Diffraction data were collected with a Bruker D8 Venture diffractometer using Mo-K_α radiation (λ = 0.7093 Å). Absorption correction was performed by the multiscan-method with the program SAINT within the Bruker APEX-II software suite[29] except for $Rb[H_2C_3N_3O_3]\cdot H_2O$-II (**2**), for which the program TWINABS[30] was employed. The structures were solved by direct methods and refined by full-matrix least-squares technique with the SHELXTL crystallographic software package.[31] The Cs/Rb/Ca/Sr/Ba, C, N and O atoms could be directly located, and the hydrogen atoms were either calculated using the AFIX 43 instruction [to the nitrogen atoms of $Sr[HC_3N_3O_3]\cdot 2H_2O$ (**10**) and $Rb[H_2C_3N_3O_3]\cdot H_2O$-II (**2**)] or assigned from the difference Fourier map and refined with restraints for the hydrogen to donor atom distance using the DFIX instruction (0.99 ± 0.1 Å for water, 0.99 ± 0.01 Å for other hydrogen atoms). Relevant crystallographic data and further details of the structure determinations are summarized in Table 2, Table 3, and Table 4.

Further details of the crystal structures investigations may be obtained from the Fachinformationszentrum Karlsruhe, 76344 Eggenstein-Leopoldshafen, Germany (Fax: +49-7247-808-666; E-Mail: crysdata@fiz-karlsruhe.de, http://www.fiz-karlsruhe.de/request for deposited data.html) on quoting the depository numbers CSD-433406 {$Rb[H_2C_3N_3O_3]\cdot H_2O$-I (**1**)}, , CSD-433398 {$Rb[H_2C_3N_3O_3]\cdot H_2O$-II (**2**)}, CSD-433399 {$Cs[H_2C_3N_3O_3]\cdot 2H_2O$ (**3**)}, CSD-433400 {$Cs[H_2C_3N_3O_3]\cdot 0.5H_2O$ (**4**)}, CSD-433405 {$Sr[H_2C_3N_3O_3]_2\cdot 4H_2O$ (**7**)}, CSD-433403 {$Sr[HC_3N_3O_3]\cdot 3H_2O$ (**8**)}, CSD-433404 {$Sr[HC_3N_3O_3]\cdot 2H_2O$ (**10**)}, CSD-433401 {$Sr_2[C_3N_3O_3]OH$ (**9**)}, and CSD-433402 {$Ba_3[H_2C_3N_3O_3]_2[HC_3N_3O_3]_2\cdot 4H_2O$ (**11**)}.

X-ray Powder Diffraction: The X-ray powder diffraction pattern was recorded with a Seifert 3003 TT diffractometer at room temperature in Bragg-Brentano geometry using Cu-K_α radiation, a GE METEOR 1D line detector, and a Ni-Filter to suppress K_β radiation (X-ray tube operated at 40 kV and 40 mA, scan range: 5–80°, increment: 0.02°, 40 scans per data point, integration time: 200 s per degree).

IR Spectroscopy: The infrared spectrum was recorded at room temperature with a Bruker EQUINOX 55 T-R spectrometer using a Plati-

Table 1. Masses (volumes), purity and supplier of the chemicals employed during the syntheses of $Sr[H_2C_3N_3O_3]_2\cdot 4H_2O$ (**7**), $Ba_3[H_2C_3N_3O_3]_2[HC_3N_3O_3]_2\cdot 4H_2O$ (**11**), $Ca[HC_3N_3O_3]\cdot 3.5H_2O$ (**6**), and $Sr[HC_3N_3O_3]\cdot 3H_2O$ (**8**).

	$Sr[H_2C_3N_3O_3]_2\cdot 4H_2O$	$Ba_3[H_2C_3N_3O_3]_2[HC_3N_3O_3]_2\cdot 4H_2O$	$Ca[HC_3N_3O_3]\cdot 3.5H_2O$	$Sr[HC_3N_3O_3]\cdot 3H_2O$
$AECl_2\cdot xH_2O$	$SrCl_2\cdot 6H_2O$ (Aldrich, 99 %): 1.16 mmol / 309,8 mg	$BaCl_2\cdot 2H_2O$ (Riedel-de Haën, 99 %): 0.39 mmol / 94.6 mg	$CaCl_2\cdot 2H_2O$ (Sigma-Aldrich, 99 %): 0,77 mmol / 113.9 mg	$SrCl_2\cdot 6H_2O$ (Aldrich, 99 %): 1.16 mmol / 309,8 mg
H_2O	15 ml	5 ml	10 ml	Column 5
NaOH (AppliChem, technical grade)	2,32 mmol / 93.0 mg	1.16 mmol / 94.6 mg	2,32 mmol / 93.0 mg	4.65 mmol / 271.7 mg
Cyanuric acid (Merck, 98 %)	1.55 mmol / 200,0 mg	0.39 mmol / 50,0 mg	0,78 mmol / 100,0 mg	1.16 mmol / 150,0 mg
H_2O	15 ml	5 ml	10 ml	15 ml
NaCl (VWR Chemicals, 99 %)	4,65 mmol / 271,7 mg	4.13 mmol / 94.6 mg	3,62 mmol / 211.3 mg	4,65 mmol / 271,7 mg
H_2O	60 ml	80 ml	70 ml	60 ml

Table 2. Crystal data and structure refinements of $Rb[H_2C_3N_3O_3]\cdot H_2O$-I (**1**), $Rb[H_2C_3N_3O_3]\cdot H_2O$-II (**2**), and $Cs[H_2C_3N_3O_3]\cdot 0.5H_2O$ (**3**).

	$Rb[H_2C_3N_3O_3]\cdot H_2O$-I	$Rb[H_2C_3N_3O_3]\cdot H_2O$-II	$Cs[H_2C_3N_3O_3]\cdot 0.5H_2O$
Formula	$RbH_4C_3N_3O_4$	$RbH_4C_3N_3O_4$	$CsH_3C_3N_3O_{3.5}$
M_r /g·mol^{-1}	463.12	463.12	296.83
Crystal size /mm^3	$0.40\times0.35\times0.09$	$0.07\times0.10\times0.02$	$0.03\times0.03\times0.02$
Crystal system	triclinic	triclinic	monoclinic
Space group	$P\bar{1}$	$P\bar{1}$	$P2_1/m$
a /Å	6.792(3)	8.3222(18)	10.9064(4)
b /Å	9.749(4)	9.554(2)	16.1066(6)
c /Å	11.238(4)	9.609(2)	11.7027(4)
α /°	67.467(11)	61.035(12)	
β /°	80.178(11)	81.757(12)	100.898(2)
γ /°	72.551(11)	83.466(12)	
V /Å^3	654.8(4)	660.8(3)	2018.35(13)
Z	2	2	2
D_{calcd} /g·cm^{-3}	2.35	2.33	2.664
μ(Mo-K_α) /cm^{-1}	7.53	7.46	5.46
F(000), e	448	448	1498
hkl range	±8, ±11, ±13	±9, –8 ≤ k ≥ 10, +10	±12, ±18, ±13
$[(\sin\theta)/\lambda]_{max}$ /Å^{-1}	1.08	0.56	0.59
Refl. measured	16518	25119 (all domains)	47021
Refl. unique	2293	3789 (all domains)	3526
R_{int}	0.0882	0.0839 (all domains)	0.0938
Param. refined	223	212	325
$R(F)/wR(F^2)$ (all reflexions)	0.0071/0.0946	0.0487/0.1257	0.0701/0.0822
GoF (F^2)	1.083	1.051	1.148
$\Delta\rho_{fin}$ (max/min) /e·Å^{-3}	0.78/–0.63	1.05/–0.68	1.68/–0.96

Table 3. Crystal data and structure refinements of $Sr[H_2C_3N_3O_3]_2\cdot 4H_2O$ (**7**), $Ba_3[H_2C_3N_3O_3]_2[HC_3N_3O_3]_2\cdot 4H_2O$ (**11**), and $Ca[HC_3N_3O_3]\cdot 3.5H_2O$ (**6**).

	$Sr[H_2C_3N_3O_3]_2\cdot 4H_2O$	$Ba_3[H_2C_3N_3O_3]_2[HC_3N_3O_3]_2\cdot 4H_2O$	$Ca[HC_3N_3O_3]\cdot 3.5H_2O$
Formula	$SrH_{12}C_6N_6O_{10}$	$Ba_3H_{14}C_{12}N_{12}O_{16}$	$CaH_8C_3N_3O_5$
M_r /g·mol^{-1}	415.84	994.29	206.19
Crystal size /mm^3	$0.123\times0.082\times0.075$	$0.134\times0.075\times0.071$	$0.152\times0.127\times0.034$
Crystal system	monoclinic	triclinic	monoclinic
Space group	$P2_1/c$	$P\bar{1}$	$P2_1/c$
a /Å	6.4672(2)	6.5781(3)	7.3451(16)
b /Å	18.8613(6)	9.0411(4)	12.251(3)
c /Å	10.7532(4)	10.2008(4)	17.141(3)
α /°		91.018(2)	
β /°	91.0799(11)	91.770(3)	91.883(6)
γ /°		107.134(2)	
V /Å^3	1311.44(8)	579.24(4)	1541.6(5)
Z	4	1	4
D_{calcd} /g·cm^{-3}	2.11	2.85	1.98
μ(Mo-K_α) /cm^{-1}	4.18	5.15	0.83
F(000), e	832	466	952
hkl range	±7, ±23, ±13	±7, ±10, ±12	±8, ±13, ±18
$[(\sin\theta)/\lambda]_{max}$ /Å^{-1}	0.61	0.60	0.55
Refl. measured	24209	13700	12803
Refl. unique	2504	2042	2130
R_{int}	0.0480	0.0750	0.0866
Param. refined	245	217	292
$R(F)/wR(F^2)$ (all reflexions)	0.0746/0.1800	0.0333/0.0541	0.0670/0.0857
GoF (F^2)	1.441	1.028	0.982
$\Delta\rho_{fin}$ (max/min) /e·Å^{-3}	0.82/–1.21	0.99/–0.65	0.30/–0.28

num ATR device (scan range: 400–4000 cm^{-1}, resolution: 4 cm^{-1}, 32 scans per sample).

UV/Vis Spectroscopy: The UV/Vis spectrum was recorded as a diffuse reflection spectrum at room temperature with a Varian Cary 300 Scan UV/Vis spectrophotometer using an Ulbricht sphere detector and a deuterium lamp / mercury lamp light source (scan range: 200–800 nm, increment 1 nm, scan-rate: 600 nm·min^{-1}).

Thermogravimetry: The TG analysis was performed with a NETZSCH STA 409 PC Luxx thermobalance under N_2-atmosphere in alumina crucibles (heating rate: 5 K·min^{-1}).

Table 4. Crystal data and structure refinements of $Sr[HC_3N_3O_3]\cdot 3H_2O$ (**8**), $Sr[HC_3N_3O_3]\cdot 2H_2O$ (**10**), and $Sr_2[C_3N_3O_3]OH$ (**9**).

	$Sr[HC_3N_3O_3]\cdot 3H_2O$	$Sr[HC_3N_3O_3]\cdot 2H_2O$	$Sr_2[C_3N_3O_3]OH$
Formula	$SrH_7C_3N_3O_6$	$SrH_5C_3N_3O_5$	$SrHC_3N_3O_4$
M_r /g·mol^{-1}	268.74	250.72	318.31
Crystal size /mm^3	$0.148 \times 0.123 \times 0.099$	$0.172 \times 0.092 \times 0.076$	$0.331 \times 0.083 \times 0.056$
Crystal system	monoclinic	orthorhombic	monoclinic
Space group	$P2_1/c$	*Ima*2	*C*2/*c*
a /Å	6.5360(3)	14.4843(7)	11.4286(8)
b /Å	12.1360(5)	6.9871(3)	9.0839(6)
c /Å	18.8657(8)	6.2452(3)	12.3259(9)
β /°	96.3450(10)		103.741(2)
V /Å^3	1487.28(11)	632.03(5)	1243.01(15)
Z	4	4	8
D_{calcd} /g·cm^{-3}	2.40	2.64	3.40
μ(Mo-K_α) /cm^{-1}	7.26	8.52	17.14
F(000), e	1056	488	1184
hkl range	±7, ±14, ±22	±20, ±9, ±8	±16, ±12, ±17
$[(\sin\theta)/\lambda]_{max}$ /Å^{-1}	0.60	0.70	0.70
Refl. measured	49984	3145	16484
Refl. unique	2622	906	1815
R_{int}	0.0597	0.0266	0.0543
Param. refined	277	67	113
$R(F)/wR(F^2)$ (all reflexions)	0.0275/0.0488	0.0292/0.0634	0.0369/0.0576
GoF (F^2)	1.116	1.027	1.101
$\Delta\rho_{fin}$ (max/min) /e·Å^{-3}	0.32/–0.35	1.05/–0.68	0.70/–0.59

Supporting Information (see footnote on the first page of this article): further figures illustrating the crystal structures, powder diffraction patterns, UV VIS spectra and a table comparing vibrational frequencies; moreover, a separate short video clip was uploaded showing the crystallization of compound 10.

Keywords: Alkaline earth metals; Alkali metals; Isocyanurate; Cyanurate; Structure elucidation

References

[1] M. Kalmutzki, M. Ströbele, H.-J. Meyer, *Dalton Trans.* **2013**, *42*, 12934–12939.
[2] M. Kalmutzki, M. Ströbele, F. Wackenhut, A. J. Meixner, H.-J. Meyer, *Inorg. Chem.* **2014**, *53*, 12540–12545.
[3] M. Kalmutzki, M. Ströbele, H. F. Bettinger, H.-J. Meyer, *Eur. J. Inorg. Chem.* **2014**, 2536–2543.
[4] M. Kalmutzki, M. Ströbele, D. Enseling, T. Jüstel, H.-J. Meyer, *Eur. J. Inorg. Chem.* **2015**, 134–140.
[5] K. Dolabdjian, M. Ströbele, H.-J. Meyer, *Z. Anorg. Allg. Chem.* **2015**, 765–768.
[6] M. Kalmutzki, K. Dolabdjian, N. Wichtner, M. Ströbele, C. Berthold, H.-J. Meyer, *Inorg. Chem.* **2017**, *56*, 3357–3362.
[7] M. Kalmutzki, M. Ströbele, F. Wackenhut, A. J. Meixner, H.-J. Meyer, *Angew. Chem. Int. Ed.* **2014**, *53*, 14260–14263.
[8] F. Liang, L. Kang, X. Zhang, M.-H. Lee, Z. Lin, Y. Wu, *Cryst. Growth Des.* **2017**, *17*, 4015–4020.
[9] G. B. Seifer, *Russ. J. Coord. Chem.* **2002**, *28*, 301–324.
[10] G. S. Nichol, W. Clegg, M. J. Gutmann, D. M. Tooke, *Acta Crystallogr., Sect. B* **2006**, *62*, 798–807.
[11] T. F. Sysoeva, M. Z. Branzburg, M. Z. Gurevich, Z. A. Starikova, *J. Struct. Chem.* **1990**, *31*, 602–608.
[12] R. E. Marsh, M. Kapon, S. Huc, F. H. Herbstein, *Acta Crystallogr., Sect. B* **2002**, *58*, 62–77.
[13] Z.-B. Lin, C.-Z. Chen, D.-S. Gao, X.-Y. Huang, D. Li, *Chin. J. Struct. Chem.* **1995**, *14*, 61.
[14] A. N. Chekhlov, *Russ. J. Inorg. Chem.* **2006**, *51*, 799.
[15] L. R. Falvello, I. Pascual, M. Tomás, *Inorg. Chim. Acta* **1995**, *229*, 135–142.
[16] L. R. Falvello, I. Pascual, M. Tomás, E. P. Urriolabeitia, *J. Am. Chem. Soc.* **1997**, *119*, 11894–11902.
[17] M.-S. Liu, Z.-Y. Zhou, L.-C. Zhu, X.-X. Zhou, Y.-P. Cai, *Acta Crystallogr., Sect. E* **2007**, *63*, m2578.
[18] pK_{a1} = 6.88, pK_{a2} = 11.40, pK_{a3} = 13.50: *CRC Handbook of Chemistry and Physics* (Ed.: W. Haynes), CRC Press, New York, **2012**, p. 5–95.
[19] T. Steiner, *Angew. Chem.* **2002**, *114*, 50–80.
[20] R. Newman, R. M. Badger, *J. Am. Chem. Soc.* **1952**, *74*, 3545–3548.
[21] I. M. Klotz, T. Askounis, *J. Am. Chem. Soc.* **1947**, *69*, 801–803.
[22] E. Irran, B. Jürgens, W. Schnick, *Chem. Eur. J.* **2001**, *7*, 5372–5381.
[23] A. Sattler, W. Schnick, *Eur. J. Inorg. Chem.* **2009**, 4972–4981.
[24] D. Raschke, *Zur Untersuchung fehlgeordneter Strukturen mit dem optischen Diffraktometer OPDIRA und über die Struktur des quaternären Fluorid-Chlorids $Ba_9Cd_{13}F_{43}Cl$*, Dissertation, Stuttgart, **1985**.
[25] S. Yuan, Y. Yang, F. Chevire, F. Tessier, X. Zhang, G. Chenz, *J. Am. Ceram. Soc.* **2010**, *93*, 3052–3055.
[26] M. Krings, G. Montana, R. Dronskowski, C. Wickleder, *Chem. Mater.* **2011**, *23*, 1694–1699.
[27] X. Piao, K. Machida, T. Horikawa, H. Hanzawa, *J. Electrochem. Soc.* **2008**, *155*, J17-J22.
[28] H. S. Kim, K. Machida, T. Horikawa, H. Hanzawa, *Chem. Lett.* **2013**, *43*, 533–534.
[29] *APEX2*, Bruker AXS Inc., Madison, WI, USA, **2012**.
[30] *TWINABS*, Bruker AXS Inc., Madison, WI, USA, **2001**.
[31] G. M. Sheldrick, *Acta Crystallogr., Sect. C* **2015**, *71*, 3–8.
[32] W. Ostwald, *Z. Phys. Chem.* **1897**, *22*, 289–330.